Paper presented at the British Applied Mathematics Colloquium, Keele University, April 2006

Integrated meteorological/hydrological modelling of the Mawddach river catchment, North Wales

Graham Hall, Roger Cratchley and Sarah Johnson
School of Agricultural and Forest Sciences,
University of Wales, Bangor

ABSTRACT

The formulation of a combined meteorological and hydrological model is discussed for a mountain area where microclimate effects can produce large variations in rainfall intensity between adjacent valleys. Use of a high resolution forecasting model provides an improved rainfall input in comparison to interpolation between widely spaced raingauge sites, or interpolation from forecasts on a regional synoptic scale. A hillslope runoff module has been developed as a central interface between meteorological, groundwater and river routing components to produce an integrated system for the prediction of flood extent and depth. An algorithm is presented for the generation of soil hydrological characteristics from gridded topographic, geological and land use data. Physics schemes for open channel flow and subsurface flow through hard rock fracture zones are assessed, and models are selected which realistically simulate observed field processes of: subcritical and supercritical river flows, river bed water loss and resurgence, and enhancement of floodwater storage in forested flood plains due to vegetation-induced lateral turbulence.

INTRODUCTION

A flood prediction model is being developed for the Mawddach catchment, North Wales, where regular flood events disrupt communications and farming activities, and can cause damage to bridges, roads and buildings. The catchment extends from sea level to mountain summits over 800m, and includes large areas of forest, moorland and improved grassland. River valleys vary in cross profile from broad and shallow to deeply incised gorges. The catchment is underlain by a complex pattern of Palaeozoic sedimentary and volcanic rocks, with an additional extensive cover of poorly consolidated glacial and periglacial deposits and blanket peat.

Flood modelling involves a number of aspects (Fig.1). A range of software models is available to simulate components of this system. These employ a variety of underlying physics assumptions and mathematical representations. This study reports experiences in developing an integrated model which is consistent with field observations of hydrological processes within the study catchment.

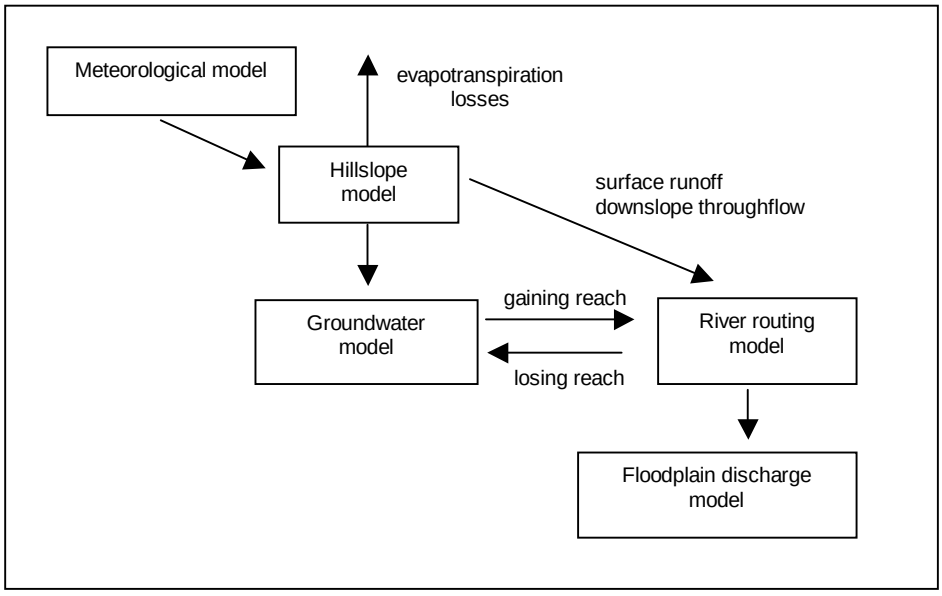

Figure 1. Integrated meteorological / hydrological model for the Mawddach catchment.

METEOROLOGICAL MODELLING

An array of 22 raingauges within the catchment has provided detailed rainfall distribution data for over 20 storm events during the period 2002 – 2005. High variability in rainfall can occur on a microclimate scale, depending on the approach directions of frontal systems and forced ascent of air masses over different mountain blocks around the catchment (figure 2).

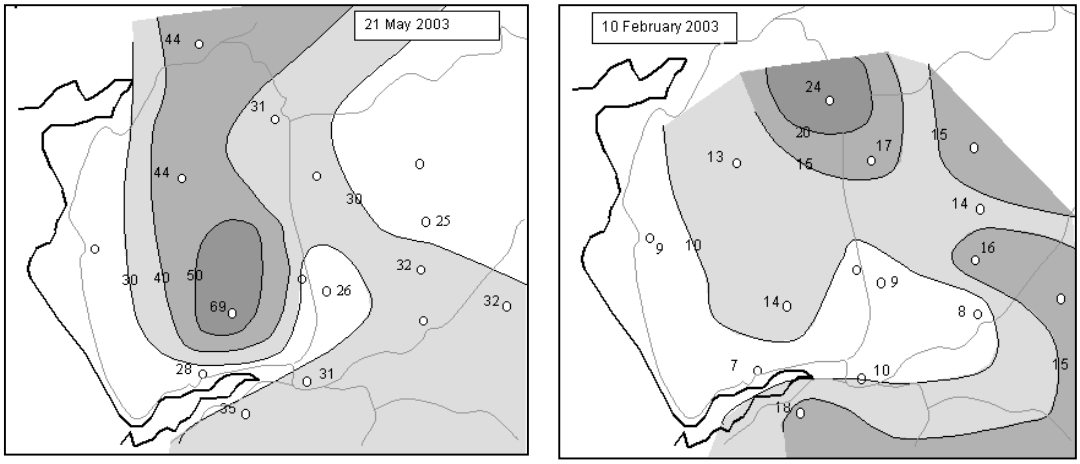

Figure 2. Examples of total storm rainfall (mm) across the Mawddach catchment.

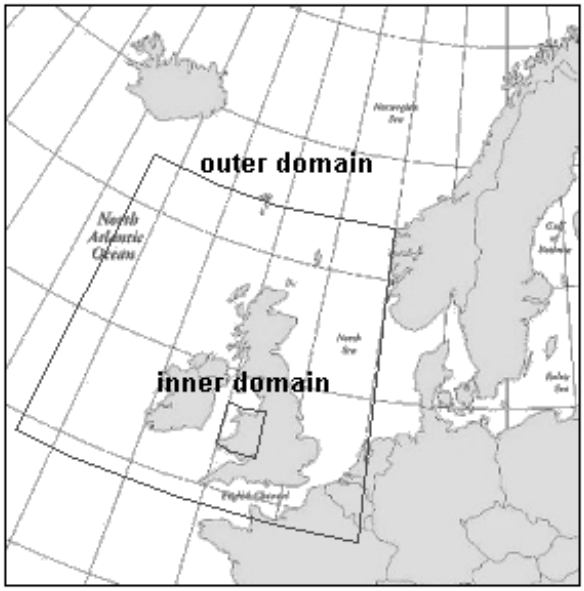

As a means of producing detailed rainfall forecasts, trials have been carried out with the MM5 meteorological modelling system developed by the US National Centre for Atmospheric Research (Grell et al., 1995). This model uses up to five nested domains of increasing grid resolution to focus on the forecast area (figure 3). The atmosphere is modelled as a series of vertical levels defined by σ coordinates, representing fixed fractions of the pressure interval between the ground surface and the model top level (figure 4). Rainfall for the Mawddach catchment is predicted on a 1km grid by the model.

Figure 3. Definition of outer and inner latitude-longitude grids.

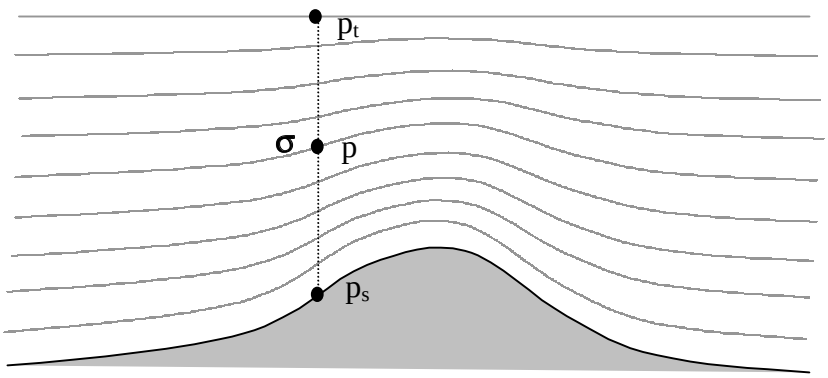

Figure 4. Definition of σ levels within the atmospheric column.

In the discussion of the mathematical model which follows, parameters and variables not specifically mentioned in the text are listed in the appendix.

Sigma levels are defined according to

$$\sigma = \frac{p - p_t}{p_s - p_t} \tag{1}$$

where p_s is the pressure at the ground surface, p_t is the pressure at the model top, and p is the pressure at level σ. The model pressure range p* is defined by

$$p^* = p_s - p_t \tag{2}$$

Changes in grid cell area can occur across the model domain due to the mapping of the curved surface of the earth onto a flat surface. This necessitates the use of a scaling factor m which for a Lambert projection is given by

$$m = \frac{\sin\psi_1}{\sin\phi}\left[\frac{\tan\phi/2}{\tan\psi_1/2}\right]^{0.716} \tag{3}$$

where $\psi_1 = 30^0$ and ψ is the colatitude ($\psi = 90^0 - \phi$).

MM5 is a non-hydrostatic model, allowing variations in pressure and temperature to develop in the vertical atmospheric profile in comparison to a constant reference state in hydrostatic equilibrium. The pressure p is related to the reference state p_0 by

$$p(x,y,z,t) = p_0(z) + p'(x,y,z,t) \tag{4}$$

where p' is the pressure perturbation. Temperature perturbation T' is similarly defined.

The model computes the changes in pressure, momentum and temperature in each grid cell at each time step. This process must allow for:

- gradients existing in the pressure, velocity and temperature fields at any moment in time,
- inflows and outflows causing variations to the pressure, velocity and temperature fields over a period of time,
- changes in pressure and temperature occurring as bodies of air change altitude, consistent with the Gas Laws,
- air flows along sigma-levels leading to changes in altitude, since a sigma-level will follow to some extent the ground surface topography.

The model is developed from a set of equations based on conservation laws involving divergence terms

$$DIV = m^2\left[\frac{\partial p^* u/m}{\partial x} + \frac{\partial p^* v/m}{\partial y}\right] - \frac{\partial p^* \dot{\sigma}}{\partial \sigma} \tag{5}$$

where the vertical velocity in σ -coordinates is

$$\dot{\sigma} = -\frac{\rho_0 g}{p^*} w - \frac{m\sigma}{p^*}\frac{\partial p^*}{\partial x} u - \frac{m\sigma}{p^*}\frac{\partial p^*}{\partial y} v \tag{6}$$

The pressure tendency is given by:

$$\frac{\partial p^* p'}{\partial t} = -m^2\left[\frac{\partial p^* up'/m}{\partial x} + \frac{\partial p^* vp'/m}{\partial y}\right] - \frac{\partial p^* p'\dot{\sigma}}{\partial \sigma} + p'DIV$$
$$- m^2 p^* \gamma p\left[\frac{\partial u/m}{\partial x} - \frac{\sigma}{mp^*}\frac{\partial p^*}{\partial x}\frac{\partial u}{\partial \sigma} + \frac{\partial v/m}{\partial y} - \frac{\sigma}{mp^*}\frac{\partial p^*}{\partial y}\frac{\partial v}{\partial \sigma}\right] \quad (7)$$
$$+ \rho_0 g\gamma p\frac{\partial w}{\partial \sigma} + p^*\rho_0 gw$$

The terms involving γ, the ratio of heat capacities (c_p/c_v) for dry air, relates to pressure changes due to cooling during vertical ascent.

Horizontal momentum (x-component) tendency is given by:

$$\frac{\partial p^* u}{\partial t} = -m^2\left[\frac{\partial p^* uu/m}{\partial x} + \frac{\partial p^* vu/m}{\partial y}\right] - \frac{\partial p^* u\dot{\sigma}}{\partial \sigma} + uDIV \quad (8)$$
$$- \frac{mp^*}{\rho}\left[\frac{\partial p'}{\partial x} - \frac{\sigma}{p^*}\frac{\partial p^*}{\partial x}\frac{\partial p'}{\partial \sigma}\right] + p^* fv + D_u$$

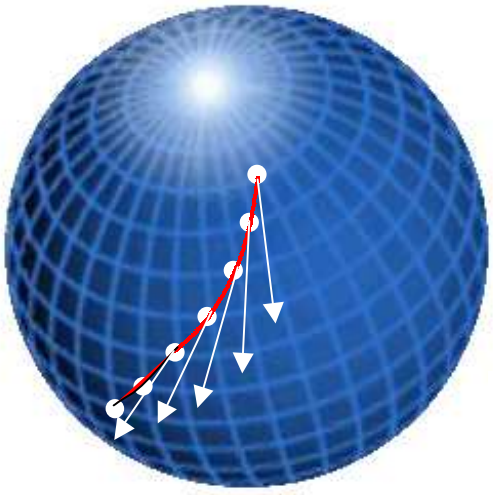

The term involving f is related to the Coriolis force. This is an imaginary force due to the rotation of the earth which appears to deflect objects to the right of their track when moving towards the Equator, or to the left of their track when moving towards the Pole in the northern hemisphere (figure 5). The D term represents diffusion and vertical mixing due to planetary boundary layer turbulence or dry convection.

Figure 5. Representation of the track of a particle moving with constant velocity above the Earth, showing an apparent deflection relative to the rotating surface.

A similar expression to the horizontal x-component momentum tendency is derived for the horizontal y-component momentum tendency.

The expression for the vertical (z-component) momentum tendency is

$$\frac{\partial p^* w}{\partial t} = -m^2\left[\frac{\partial p^* uw/m}{\partial x} + \frac{\partial p^* vw/m}{\partial y}\right] - \frac{\partial p^* w\dot{\sigma}}{\partial \sigma} + wDIV \quad (9)$$
$$+ p^* g\frac{\rho_0}{\rho}\left[\frac{1}{p^*}\frac{\partial p'}{\partial \sigma} + \frac{T_v^{'}}{T} - \frac{T_0 p'}{Tp_0}\right] - p^* g\left[(q_c + q_r)\right] + D_w$$

The terms involving T relate to volume changes during heating or cooling during vertical motions, and the term involving q_c and q_r relate to the vertical motion of water in the form of cloud and rain.

The temperature tendency is

$$\frac{\partial p^* T}{\partial t} = -m^2\left[\frac{\partial p^* uT/m}{\partial x} + \frac{\partial p^* vT/m}{\partial y}\right] - \frac{\partial p^* T\dot{\sigma}}{\partial \sigma} + T.DIV + \frac{1}{\rho c_p}\left[p^* \frac{Dp'}{Dt} - \rho_0 g p^* w - D_{p'}\right] + p^* \frac{\dot{Q}}{c_p} + D_T \quad (10)$$

Terms involving c_p are derived from the first law of thermodynamics and determine pressure changes due to heating and cooling during vertical motions (Jacobson, 1999).

A finite difference scheme is used with equations (8) to (10) to model the progression of pressure, momentum and temperature across the modelling domain. At intervals, values for these parameters can be supplied at the outer boundary. Cells within the outer rows of the model will then be progressively nudged towards the boundary values, to avoid the model diverging from observations over an extended simulation period.

A central function of the MM5 model in its hydrological application is the determination of rainfall rates on a high resolution grid scale. Moisture and precipitation are handled by the determination of three mixing ratios:

Water vapour mixing ratio

$$\frac{\partial p^* q_v}{\partial t} = -m^2\left[\frac{\partial p^* uq_v/m}{\partial x} + \frac{\partial p^* uq_v/m}{\partial y}\right] - \frac{\partial p^* q_v\dot{\sigma}}{\partial \sigma} + \delta_{nh} q_v DIV + p^*\left(-P_{RE} - P_{CON} - P_{II} - P_{ID}\right) + D_{qv} \quad (11)$$

Cloud water mixing ratio

$$\frac{\partial p^* q_c}{\partial t} = -m^2\left[\frac{\partial p^* uq_c/m}{\partial x} + \frac{\partial p^* uq_c/m}{\partial y}\right] - \frac{\partial p^* q_c\dot{\sigma}}{\partial \sigma} + \delta_{nh} q_c DIV + p^*\left(P_{ID} + P_{II} - P_{RC} - P_{RA} + P_{CON}\right) + D_{qc} \quad (12)$$

Rain water mixing ratio

$$\frac{\partial p^* q_r}{\partial t} = -m^2\left[\frac{\partial p^* uq_r/m}{\partial x} + \frac{\partial p^* uq_r/m}{\partial y}\right] - \frac{\partial p^* q_r\dot{\sigma}}{\partial \sigma} + \delta_{nh} q_r DIV - \frac{\partial V_f \rho g q_r}{\partial \sigma} + p^*(P_{RE} + P_{RC} + P_{RA}) + D_{qr} \quad (13)$$

These equations include a range of physical processes involving water phase conversion: P_{RE} is evaporation of rain drops, P_{CON} is condensation of water vapour, P_{II} is initiation of ice crystals, P_{ID} is deposition of vapour onto ice crystals, P_{RC} is conversion of cloud drops to rain drops, P_{RA} is accretion of cloud drops by rain drops.

The basic model provides for condensation whenever relative humidity reaches 100%, with subsequent production of raindrops and fallout under gravity. The model successfully handles seeder-feeder mechanisms, where raindrops produced in high cloud layers fall

through lower saturated air and increase their volume. Advection of raindrops during descent to the ground surface is also handled correctly.

Rain accretion rate is calculated from

$$P_{RA} = \frac{1}{4}\pi\rho a q_c E N_0 \frac{\Gamma(3+b)}{\lambda^{3+b}} \tag{14}$$

where parameter **a** has a value of 842.99 for rain or 11.72 for snow, parameter **b** has a value of 0.8 for rain or 0.41 for snow, and Γ is the gamma- function. The parameter $N_0 = 8 \times 10^6$ for rain, 2×10^7 for snow.

The fall speed of rain is calculated from

$$V_f = a\frac{\Gamma(4+b)}{6}\lambda^{-b} \tag{15}$$

where

$$\lambda = \left(\frac{\pi N_0 \rho_w}{\rho q_r}\right)^{1/4} \tag{16}$$

The modelling system has proved to be very effective in determining rainfall rates for 1 hour time steps during winter frontal storm events over the Mawddach catchment. The extent of nimbus stratus clouds is realistically modelled (figure 6), and precipitation is within 10% agreement with gauging stations across the study area.

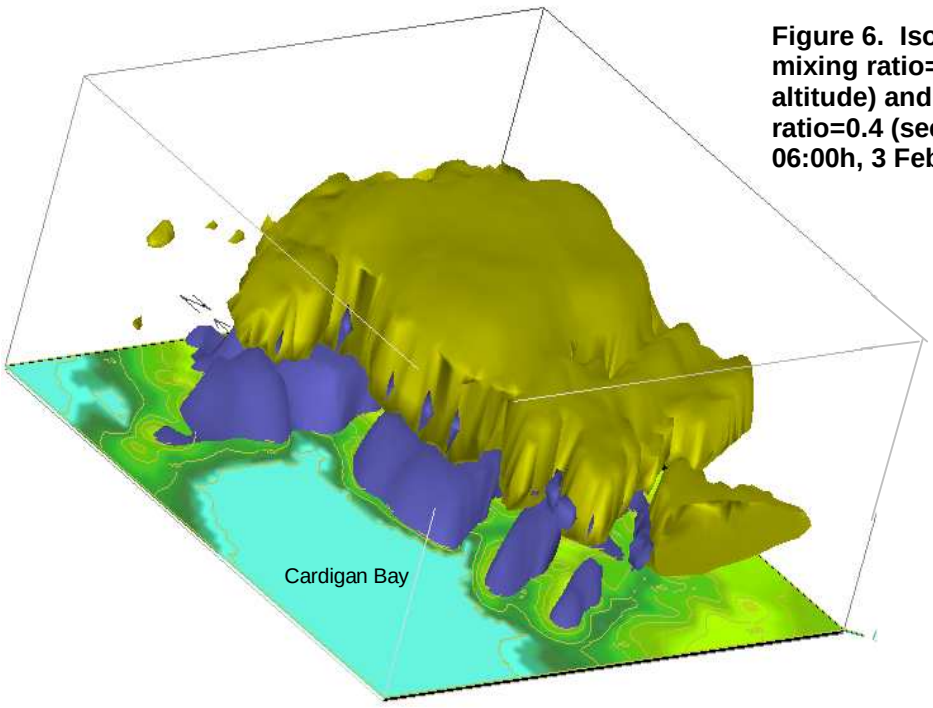

Figure 6. Isosurfaces for cloud mixing ratio=0.4 (seen at higher altitude) and precipitation mixing ratio=0.4 (seen at lower altitude). 06:00h, 3 February 2004.

Modelling of summer thunderstorm events presents a greater modelling challenge, where vertical convective motions are dominant. MM5 offers a series of cumulus parameterisation schemes to model convective rainfall generation. The principle of cumulus parameterisation is that convective motion can take place on a scale smaller than a model grid cell. Whilst the mean relative humidity within a cell may not reach 100%, there may be zones within the cell

where water vapour is concentrated and condensation may occur (figure 7). Condensation will produce rainfall, but also releases latent heat which can drive upward convection.

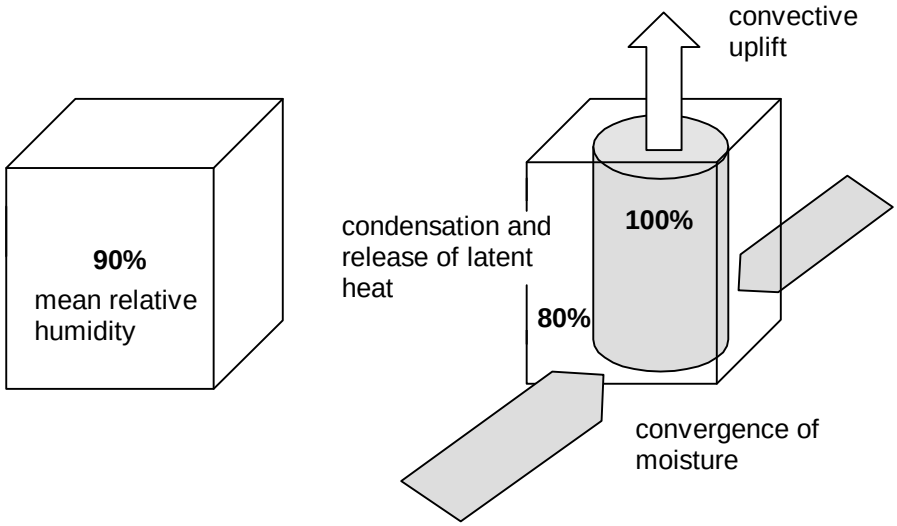

Figure 7: Principles of the Anthes-Kuo cumulus parameterisation scheme

The simplest cumulus parameterisation is the Anthes-Kuo scheme. This algorithm estimates the rate of convergence of moisture at the boundaries of a grid call. If moisture convergence is above a threshold value, the temperatures for grid cells in the overlying vertical air column are checked to determine if convection is possible. The base and top level of cloud is then determined, and vertical air motion computed. A theoretical temperature function within the convecting column is used to calculate condensation and rainfall production.

For the Anthes-Kuo model, the temperature tendency equation (10) is modified to include a term M_t

$$\frac{\partial p^* T}{\partial t} = -m^2\left[\frac{\partial p^* uT/m}{\partial x} + \frac{\partial p^* vT/m}{\partial y}\right] - \frac{\partial p^* T\dot{\sigma}}{\partial \sigma} + T.DIV \qquad (17)$$
$$+ \frac{1}{\rho c_p}\left[p^* \frac{Dp'}{Dt} - \rho_0 g p^* w - D_{p'}\right] + p^* \frac{L_v}{c_{pm}} N_h(\sigma)(1-b) g M_t + D_T$$

where M_t is the vertically integrated moisture convergence:

$$M_t = \left(\frac{m^2}{g}\right)\int_0^1 \frac{\nabla p^* \dot{V} q_v}{m} d\sigma \qquad (18)$$

The equation for tendency in water vapour mixing ratio (11) is similarly modified:

$$\frac{\partial p^* q_v}{\partial t} = -m^2\left[\frac{\partial p^* uq_v/m}{\partial x} + \frac{\partial p^* uq_v/m}{\partial y}\right] - \frac{\partial p^* q_v\dot{\sigma}}{\partial \sigma} + \delta_{nh} q_v DIV \qquad (19)$$
$$+ p^*(-P_{RE} - P_{CON} - P_{II} - P_{ID}) + p^* bg M_t N_m(\sigma) + p^* V_{qf}(\sigma) + D_{qv}$$

A major flood event in July 2001 caused extensive damage in the Mawddach catchment. Exceptionally intense rainfall occurred from a convective supercell within a squall line across the region (Mason, 2002).

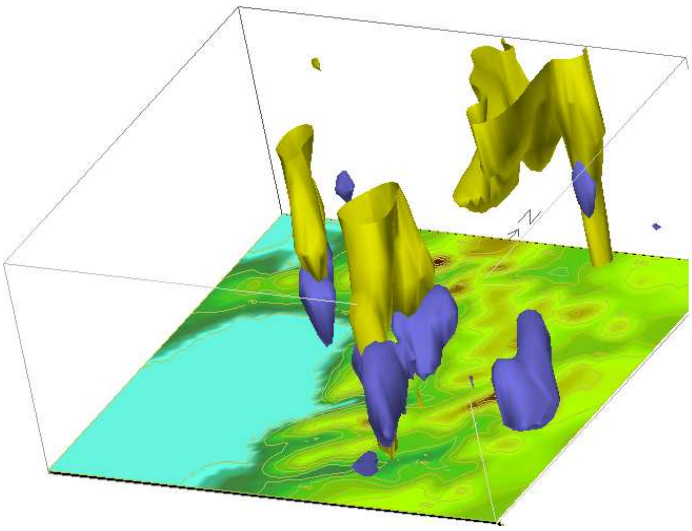

Figure 8: Isosurfaces for cloud mixing ratio=0.4 (extending to higher altitude) and precipitation mixing ratio=0.4 (seen at lower altitude). 18:00h, 3 July 2001. Anthes-Kuo model.

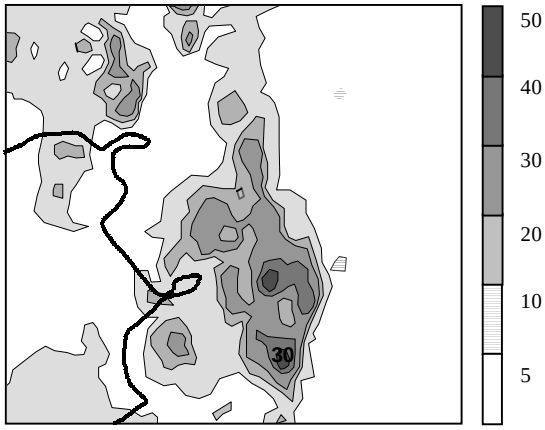

Figure 9: One hour rainfall total. 18:00h-19:00h, 3 July 2001. Anthes-Kuo model.

Modelling of the July 2001 flood event was first carried out using the basic MM5 system with no cumulus physics scheme. Rainfall generated was less than 20% of the raingauge data, and the model would have been ineffective for flood forecasting. A second run was carried out with Anthes-Kuo cumulus parameterisation, and results accurately reproduced the form of the squall line (figures 8-9). Towering convective clouds were correctly modelled, with localised rainfall intensities reaching a maximum of 40mm/hour which is in close agreement with field data (Hall and Cratchley, 2006).

An alternative convective scheme within the MM5 system is Grell cumulus parameterisation. This is a more sophisticated scheme in which individual clouds are modelled, along with the mechanisms of rainfall generation within them (figure 10).

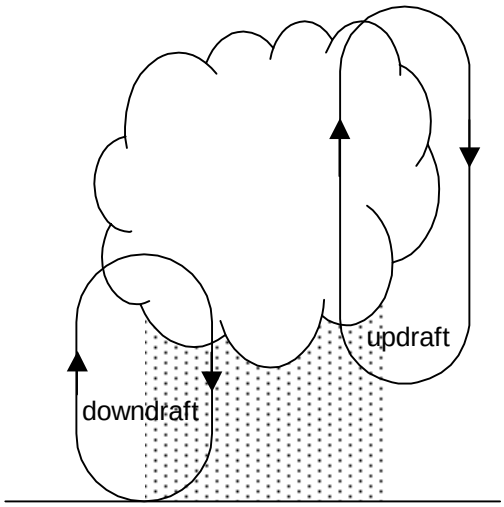

Figure 10: Air movements within a cloud, modelled by the Grell cumulus scheme.

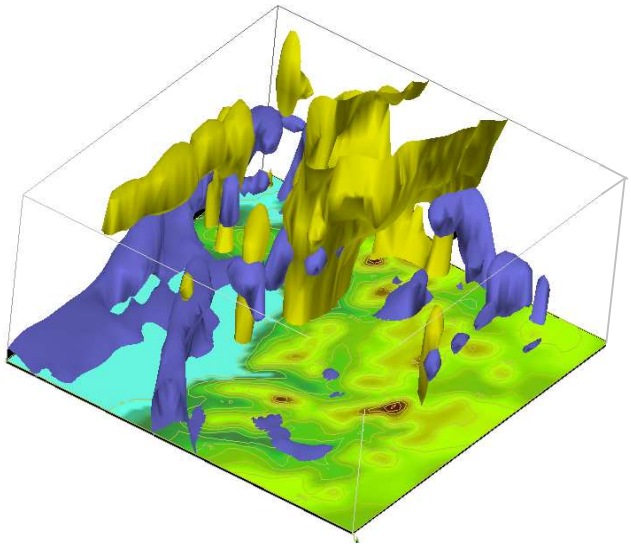

Figure 11: Isosurfaces for cloud mixing ratio=0.4 (extending to higher altitude) and precipitation mixing ratio=0.4 (seen at lower altitude). 18:00h, 3 July 2001. Grell scheme.

Simulation of the July 2001 Mawddach flood event was carried out using the Grell scheme. In comparison to the Anthes-Kuo parameterisation, a much larger amount of cumulus activity is simulated (figure 11), but the rainfall rates predicted were less than 40% of observed values. Spatial distribution of storm rainfall was also less accurate than for the Anthes-Kuo model, with the linear pattern of convective cells in the squall line not distinguished.

For the particular conditions of the July 2001 storm, the Anthes-Kuo scheme was the preferred convective scheme. Further research is necessary to determine whether this rainfall forecasting choice is appropriate for all major summer thunderstorms over the region.

HILLSLOPE MODEL

Rainwater reaching the ground will infiltrate vertically or run-off laterally at the surface or at shallow depth, depending on soil physical properties and antecedent moisture conditions.

Within the Mawddach catchment, soil characteristics vary widely. Major controlling factors are the underlying geology, position in relation to the hillslope, and type of vegetation cover.

A sequence of soil types is typically developed down a hillslope, with drier soils at higher levels where downslope drainage is rapid and upslope contributing area is small (figure 12). By contrast, wetter soils develop at the bases of hillslopes where drainage is often slower and the upslope contributing area is large. A quantitative index of wetness at any point is given by the Kirkby index (Bevan, 1997)

$$\ln (a / \tan \beta) \qquad (20)$$

where a is upslope contributing area and β is slope angle.

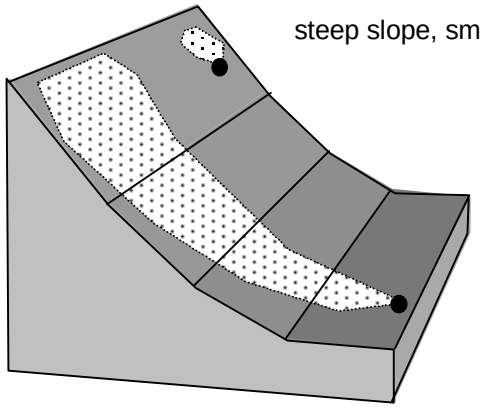

Figure 12: Factors determining Kirkby wetness index

Field investigations have shown that thick soils gradually develop on hillslopes beneath both deciduous and coniferous forest, reaching their maximum thickness as the woodland becomes mature after 30 years. Forest soils can be rapidly eroded after clear felling (Hall and Cratchley, 2005). An example is given in figures 13 and 14 where clear felling led to the loss of over 1m of soil in two years.

Water flow in soil is governed by the Darcy equation for porous media:

$$\frac{\partial}{\partial x}\left(K_x \frac{\partial h}{\partial x}\right)+\frac{\partial}{\partial y}\left(K_y \frac{\partial h}{\partial y}\right)+\frac{\partial}{\partial z}\left(K_z \frac{\partial h}{\partial z}\right)-W = S\frac{\partial h}{\partial t} \qquad (21)$$

where h terms refer to hydraulic head, K parameters are hydraulic conductivities, W is a sink and source term, and S is water storage.

Figure 13. Thick soil profile beneath forestry at Hermon, Coed y Brenin

Figure 14. Reduced soil profile thickness beneath a clear felled hillslope at Hermon

Hydraulic conductivity of the soil is not constant, but varies greatly with effective saturation. Conductivity values fall rapidly to low levels as soils dry, and pore water is retained increasing strongly by capillary forces. An equation has been proposed by van Genuchten for the calculation of soil conductivity as a function of effective saturation, depending on a parameter m related to soil texture. Typical values of m are 0.274 for coarse sandy soil, down to 0.094 for fine silty soil. The van Genuchten equation is:

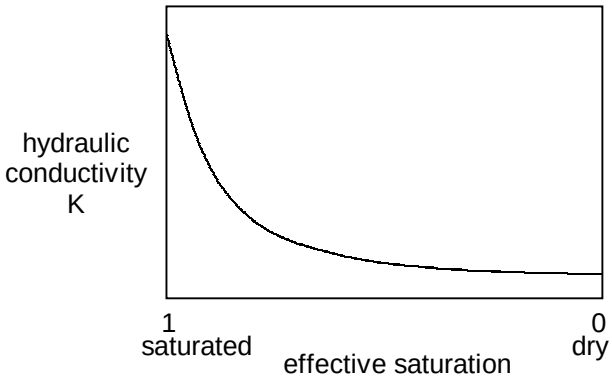

Figure 15. Relationship between soil conductivity and effective saturation

$$\frac{K(\theta)}{K_s} = \left(\frac{\theta - \theta_r}{\theta_s - \theta_r} \right)^{1/2} \left[1 - \left(1 - \left\{ \frac{\theta - \theta_r}{\theta_s - \theta_r} \right\}^{1/m} \right)^m \right]^2 \qquad (22)$$

where θ is soil moisture content, subscript s refers to moisture content at saturation, and r refers to soil water retained when the soil is dry.

A soil classification found useful for hydrological modelling is the HOST (Hydrology of Soil Types) system developed by the Institute of Hydrology (Boorman et al., 1995). An automated mapping algorithm has been developed to allocate HOST soil classes to each 50m grid square of the Mawddach catchment. This algorithm uses gridded GIS data for Kirkby wetness index, geology and land use (figure 16). Allocations to soil classes have been checked by field observations, and corrections to the map were made where necessary.

Each HOST soil class is found to have characteristic properties of texture and depth for the topsoil and subsoil layers. This in turn allows the allocation of van Genuchten m parameters for use in the calculation of hydraulic conductivity during runs of the hydrological model.

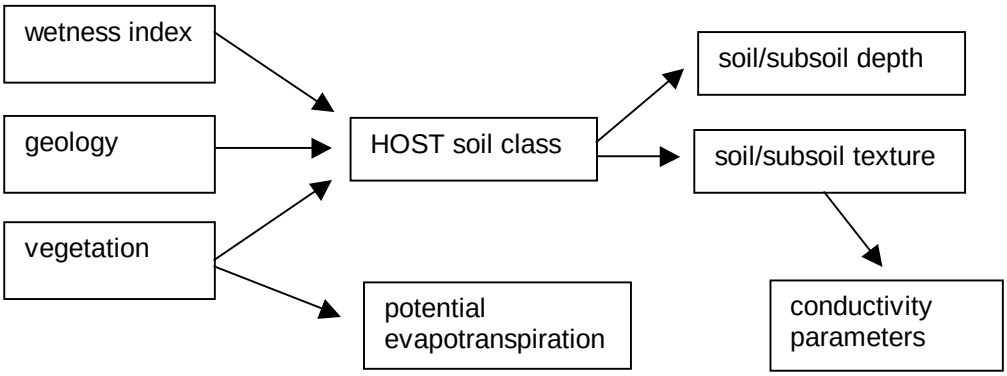

Figure 16. Determination of parameters for the hillslope model

The hillslope model determines surface runoff and throughflow which is able to enter the river system. Eight experimental sites have been established in the Mawddach catchment to monitor surface runoff and throughflow in the upper 1.5m of soil, as a means of validating the model output (figure 17).

Figure 17. Runoff and soil throughflow monitoring site, Pared yr Ychain

The volume of rainfall over areas of vegetation can be reduced by processes of evapotranspiration, which include the release of water vapour from leaf pores and direct evaporation from leaf surfaces.

Evapotranspiration rate is dependent on both climatic factors and the surface characteristics of the vegetation. Rate of water loss λE can be estimated by the Penman-Monteith equation:

$$\lambda E = \frac{\Delta_e H + \rho_a c_p \left(e_s(T_z) - e_z\right)/r_a}{\Delta_e + \gamma\left(1 + r_c/r_a\right)} \qquad (23)$$

where the $\Delta_e H$ term is related to insolation heat flow, T_z is the temperature at the surface of the tree canopy, e_s is the saturation vapour pressure at this temperature, and e_z is the actual vapour pressure at the vegetation canopy. Thus it can be seen that to use the equation, data is needed for temperature, relative humidity and incoming solar radiation at the vegetation canopy level. The parameters r_c and r_a are resistance coefficients which are characteristic of different vegetation types. Values of r are predicted to be inversely proportional to wind speed, so evapotranspiration rate increases with wind speed above the vegetation canopy.

Work is currently underway to incorporate evapotranspiration into the hillslope model using meteorological data from the MM5 mesoscale model, and to carry out a sensitivity analysis to determine the extent to which effective rainfall is reduced by evapotranspiration losses during storm events. This may be significant where wind speeds are high.

RIVER ROUTING

River channels of widely differing character make up the Mawddach system (figure 18). Flows occur under a mixture of critical and subcritical regimes, necessitating the modelling of varying water velocity-depth relations within individual reaches.

Figure 18. The River Mawddach in Coed Y Brenin, showing a transition from fast shallow supercritical flow in the middle distance, to slow deep sub-critical flow in the foreground.

The software package GSTARS (Generalized Stream Tube model for Alluvial River Simulation) produced by the US Bureau of Reclamation (Yang and Simões, 2000) has proved successful in handling mixed flow regimes. This program can be described as a one-and- a-half dimensional model, since river flow is determined from a finite number of specified cross sections (figure 19).

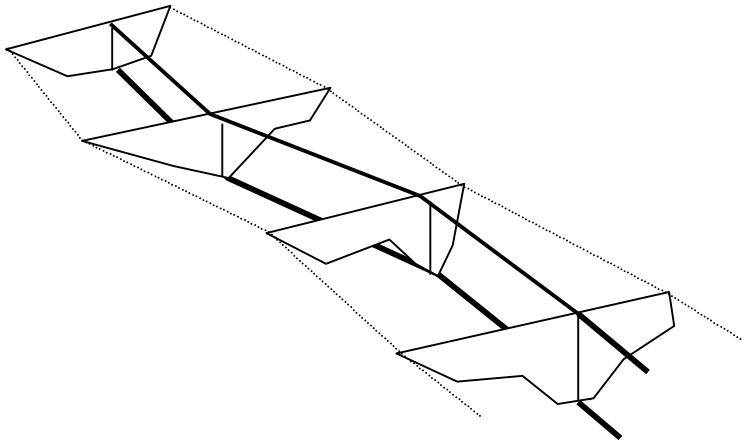

Figure 19. Schematic representation of the GSTARS model, with river flows determined from channel cross sections and river bed elevations at specified points

GSTARS is based on the energy equation:

$$z + Y + \alpha \frac{V^2}{2g} = H \qquad (24)$$

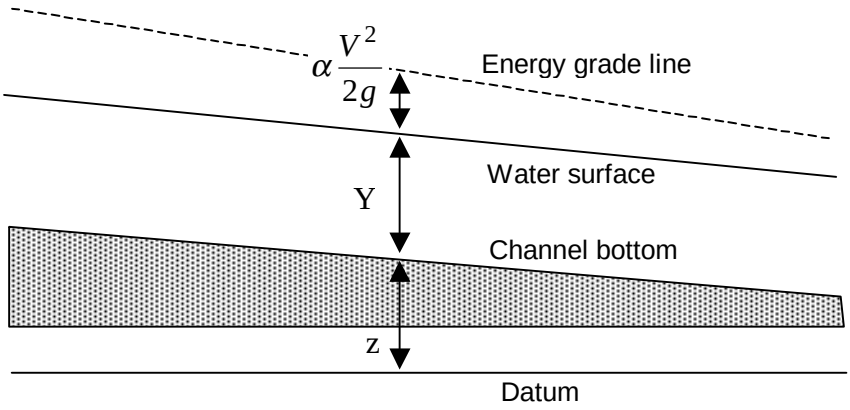

Figure 20. Components of the energy equation (24)

H is the total energy at a point in the river, expressed as a hydraulic head above a datum line. This is made up of three components: z is the height of the riverbed above the datum, Y is the water depth, and the term involving velocity V represents additional kinetic energy of the moving water (fig 20). The term α is a correction factor close to 1, which allows for a slight error due to boundary effects when the discharge is calculated as a simple product of cross sectional area and average velocity.

It is possible to calculate two values, the *normal depth* and the *critical depth*, at points in the channel. By comparing these values, it can be determined whether flow will be subcritical or supercritical under prevailing conditions. This in turn will determine whether flow will be deep and slow, or shallow and fast, for the given discharge. Where normal depth is less than critical depth, flow will be supercritical; otherwise flow will be subcritical.

Critical depth is given by the expression

$$f(D) = 1 - \alpha(D)\frac{Q^2 W(D)}{gA^3(D)} = 0 \qquad (25)$$

where f, the Froude number, has a value of 1 at critical depth. Q is discharge, W is channel width and A is cross sectional area when the water depth is D.

Normal depth is determined from

$$g(D) = Q - K(D)\sqrt{S_0} = 0 \qquad (26)$$

where S_0 is the bottom slope of the channel. K is conveyance, and is related to the flow resistance of the channel by Manning's formula

$$K = \frac{1.49}{n} AR^{2/3} \qquad (27)$$

where A is channel cross sectional area, R is hydraulic radius obtained by dividing area by wetted perimeter. Manning's Roughness Coefficient, n, is related to the characteristics of the channel and has been determined for a wide variety of river sites. Values range from 0.01 for smooth concrete-lined channels, to over 0.07 for sluggish, weedy reaches.

Storm events within the Mawddach catchment can cause rapid changes in channel profile through sediment erosion and deposition (figure 21), which in turn can affect discharge and flow velocity. The GSTARS software can predict and incorporate such changes during a flood simulation.

Figure 21. Confluence of the Mawddach and its main tributary, the River Wnion. This area of unstable gravel banks is susceptible to rapid profile changes during flood events

Sediment transport is governed by a continuity equation

$$\frac{\partial Q_s}{\partial x} + \eta \frac{\partial A_d}{\partial t} + \frac{\partial A_s}{\partial t} - q_s = 0 \qquad (28)$$

where the Q_s term represents the downstream change in sediment discharge, the term in A_d is the rate of change of sediment volume on the stream bed, the A_s term is the rate of change of suspended sediment concentration, and q_s is sediment inflow.

A selection of transport formulae are available within the GSTARS package for determining the volumes of sediment which can be carried downstream under prevailing flow conditions, and thus the rates of bed or bank erosion and accretion can be determined.

A principle of minimisation of stream energy is used to determine whether deepening or widening of the channel should occur in erosional regimes, or whether shallowing or narrowing should occur in depositional regimes. This involves minimising the integral for total stream energy

$$\Phi_T = \int \gamma Q S dx \qquad (29)$$

along the length of the river reach, where Q is discharge and S is the downstream slope of the river bed. the constant γ is the specific weight of water. The function will predict widening of the channel where gradients are small, but deepening of the channel where gradients are steep.

FLOOD PREDICTION

Detailed determination of the aerial extent and depth of flooding requires the use of a land surface model employing finite element or finite difference methods for water flows.
The RIVER-2D software produced by the University of Alberta has been used for this purpose (Steffler and Blackburn, 2002). The model has been evaluated by comparison with historical flood data for areas of the Mawddach catchment within the Coed y Brenin Forest (figure 21).

Figure 22. Flood modelling area at Cefn Deuddwr, Coed y Brenin

The governing equation for the RIVER-2D program is the conservation of water mass:

$$\frac{\partial H}{\partial t} + \frac{\partial q_x}{\partial x} + \frac{\partial q_y}{\partial y} = 0 \qquad (30)$$

where the term in H refers to the rate of change in hydraulic head as river level changes, and the terms in q are the discharge gradients in the coordinate directions x and y.

Changes to the boundary geometry of the river channel will occur as the water surface extends during flood events. This can cause instability in a finite element model, but is successfully handled in the River2D modelling code by linking river levels to the groundwater profiles below adjacent hillslopes. Beyond the channel margins, equation (30) is replaced by a groundwater equation

$$\frac{\partial H}{\partial t} = \frac{T}{S}\left(\frac{\partial^2}{\partial x^2}(H + z_b) + \frac{\partial^2}{\partial y^2}(H + z_b) \right) \qquad (31)$$

in which T is transmissivity, a measure of the rate at which water can permeate through the geological formation, S is the storativity which determines the volume of water which can be held within a unit volume of the rock material, and z_b is the ground surface elevation.

Modelling has been carried out to simulate the effects of a flood event in July 2001 which affected the area shown in figure 22 above. The maximum extent of flood plain inundation is consistent with field evidence of flood debris accumulation (figure 23).

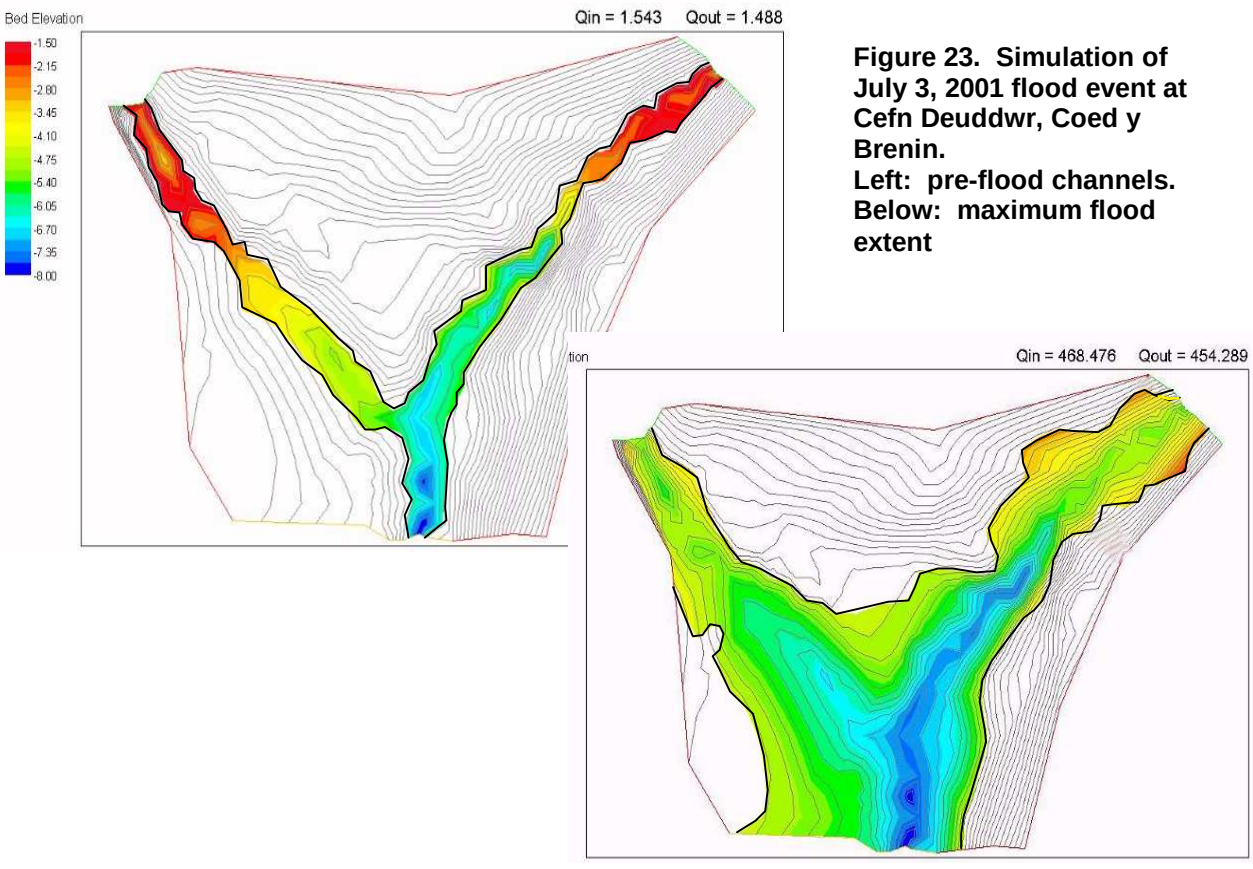

Figure 23. Simulation of July 3, 2001 flood event at Cefn Deuddwr, Coed y Brenin.
Left: pre-flood channels.
Below: maximum flood extent

RIVER-2D offers opportunities to investigate the effects of flood plain forestry in enhancing temporary water storage and reducing flood peaks downstream. The model incorporates an eddy viscosity coefficient ν_t which is used in simulating turbulent shear stresses according to the relation

$$\tau_{xy} = \nu_t \left(\frac{\partial U}{\partial y} + \frac{\partial V}{\partial x} \right) \tag{32}$$

The eddy viscosity coefficient is made up of three components

$$\nu_t = \varepsilon_1 + \varepsilon_2 \frac{H\sqrt{U^2 + V^2}}{C_s} + \varepsilon_3^2 H^2 \sqrt{2\frac{\partial U}{\partial x} + \left(\frac{\partial U}{\partial y} + \frac{\partial V}{\partial x} \right)^2 + 2\frac{\partial V}{\partial y}} \tag{33}$$

The ε_1 term is a constant, the ε_2 term represents a bed shear. The key variable is the $\varepsilon 3$ term, representing transverse shear which will be high for water flows through flood plain forestry but low for unimpeded flows across meadow floodplain. Using appropriate values for ε_3, it is estimated that dense woodland can increase water depth on the floodplain by up to a metre in comparison to grassland, with consequent increase in transient storage.

GROUNDWATER-RIVER INTERACTIONS

From fieldwork within the Mawddach catchment, it has become apparent that groundwater-river interactions are important in the mechanisms generating floods. Many of the main valleys are infilled by thick glacial and periglacial deposits (figure 24). Flooding generally occurs after a period of several days of heavy rainfall which saturates these deposits, developing extensive surface runoff areas.

Figure 24. Deposits of glacial and periglacial clays, sands, gravels and boulder beds infilling the Afon Wen valley to a depth of more than 8 metres.

Groundwater movements through permeable strata can be modelled by the MODFLOW finite difference package, based on the Darcy continuity equation

$$\frac{\partial}{\partial x}\left(K_x \frac{\partial h}{\partial x} \right) + \frac{\partial}{\partial y}\left(K_y \frac{\partial h}{\partial y} \right) + \frac{\partial}{\partial z}\left(K_z \frac{\partial h}{\partial z} \right) - W = S \frac{\partial h}{\partial t} \tag{34}$$

where K values are hydraulic conductivities of pore water through the permeable material, terms in h are gradients in hydraulic head, W is a term allowing for sources and sinks of water within a model cell, and the term in S relates to storage of water within a cell.

Main river valleys within the Coed y Brenin Forest area of the catchment are generally aligned along bedrock fracture zones in Palaeozoic volcanic rocks and hard sedimentary strata. Experiments have been carried out using electronic temperature probes inserted in river bed gravels, which indicate resurgence of groundwater from high conductivity fractures in the river bed during flood events (figures 25 and 26).

Figure 25(a). Left: Afon Wen valley, aligned along the Afon Wen fault. During dry conditions, water flows can be very low due to loss to groundwater through river bed fractures

Figure 25(b). Right: Installing temperature probes in riverbed gravels

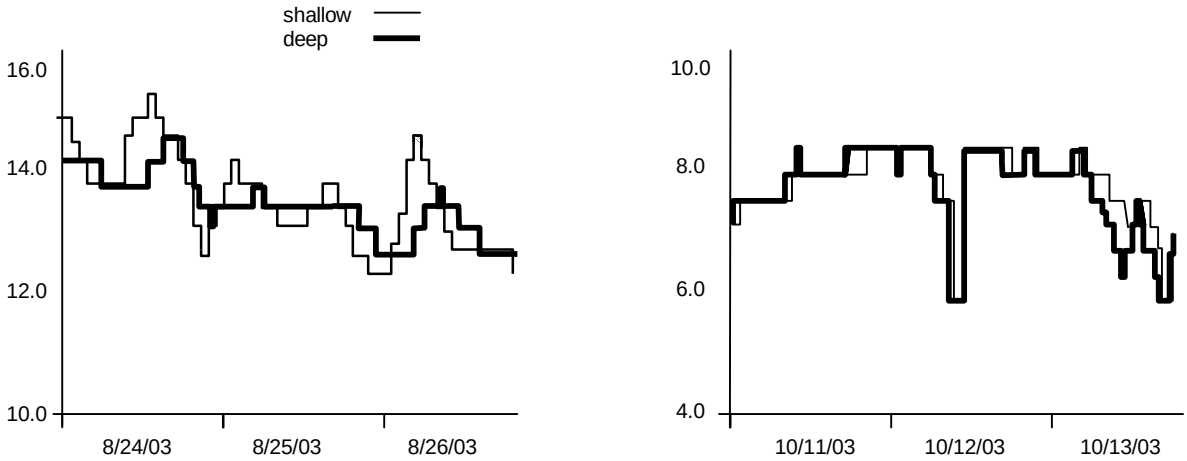

Figure 26. Riverbed temperatures in the Afon Wen. The shallow thermometer is located at the sediment surface, and the deep thermometer at a depth of 1.5m in river gravels. Under low flow conditions, river water seeps downwards to groundwater store, showing a deep temperature response some 6 hours after surface temperature changes. In flood conditions, the flow is reversed, with changes in deep sediment temperature reflected in surface temperature changes around 2 hours later.

The normal application of the MODFLOW groundwater model is to determine flows through permeable strata such as sands (figure 27(a)).

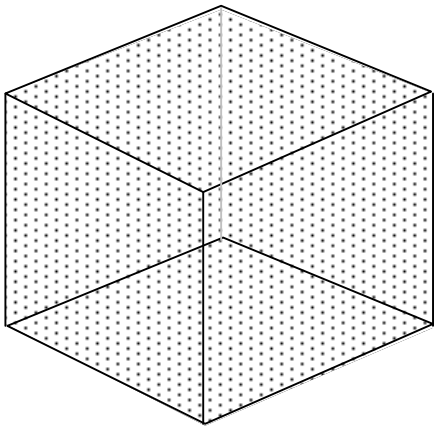

Figure 27(a). Theoretical model of permeable material with interconnecting pore spaces.

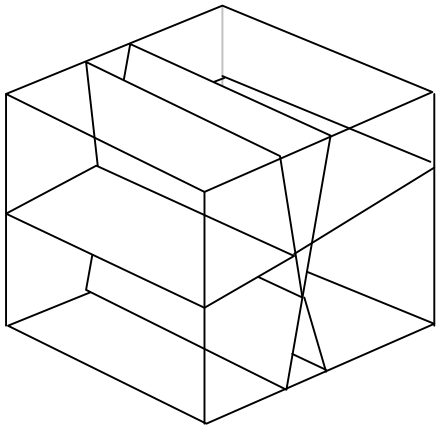

Figure 27(b). Theoretical model of fractured impermeable material with groundwater flow planes intersecting cell boundaries

Svensson (2001) has proposed an adaption to the model which instead treats the permeable medium as a solid substrate intersected by a fracture system connecting the faces of cells. Flow through the cell is determined from

$$Q = K\Delta h \sum \frac{HW}{L} \tag{35}$$

where a sum is obtained of the height (H), width (W) and length (L) dimensions of fractures intersecting the cell boundaries. Svensson assumes a constant thickness h and hydraulic conductivity K for fracture planes. This approach is being investigated further as a means of modelling water flows within the Mawddach fault zones.

DISCUSSION

Meteorological and hydrological modelling have historically been treated as separate disciplines, and limited work has been done in developing integrated systems. Hydrological modelling packages have typically generated rainfall distributions by linear interpolation between sparse rain gauge sites, or by applying an altitude function over mountains to enhance raingauge data collected at valley locations. Neither of these approaches is entirely satisfactory for a mountain region such as the Mawddach catchment, where microclimate effects can lead to variations in rainfall between adjacent valleys by up to a factor of 3. The improved accuracy of rainfall distributions provided by the MM5 mesoscale model results in improved predictive capabilities of the hydrological model.

A wide range of hydrological models has been published, ranging from catchment scale models generating hydrographs from regionally averaged runoff characteristics, to specialised models for particular components of the hydrological cycle such as groundwater flows or river routing. From experience of modelling in the Mawddach catchment, it appears that a realistic system can be developed by linking a series of specialist programs whose theoretical bases are consistent with the observed mechanisms of flood generation in the catchment. A process model of this type should be valuable in determining the effects of catchment management changes, such as development or removal of forestry, or engineering works affecting river banks and flood plains.

REFERENCES

Beven K.J., 1997. Distributed hydrological modelling. Wiley.

Boorman D.B., Hollis J.M. and Lilly A., 1995. Report No.126. Hydrology of soil types: a hydrologically-based classification of the soils of the United Kingdom. Institute of Hydrology.

Calvert J., 2006. Open-Channel Flow. University of Denver. www.du.edu/~jcalvert/tech/fluids/opench.htm.

Grell G.A., Dudhia J. and Stauffer D.R., 1995. A description of the Fifth-generation Penn State/NCAR Mesoscale Model (MM5). NCAR Technical Note TN-398 + STR. National Centre for Atmospheric Research, Boulder, Colorado.

Hall G. and Cratchley R., 2005. The role of forestry in flood management in a Welsh upland catchment. Proceedings of the 45th Congress of the European Regional Science Association, Amsterdam.

Hall G. and Cratchley R., 2006. Sediment erosion, transport and deposition during the July 2001 Mawddach extreme flood event *in* 'Sediment dynamics and the hydromorphology of fluvial systems', A. Werritty (ed.), IAHS (in press).

Jacobson M.Z., 1999. Fundamentals of Atmospheric Modelling. Cambridge University Press.

Mason, J., 2002. The July 2001 thunderstorms and their catastrophic effects in Mid-Wales. www.geologywales.co.uk/storms

McDonald M.G. and Harbaugh A.W., 1988. A modular three-dimensional finite-difference groundwater flow model. U.S. Geological Survey. Denver, Colorado.

National Centre for Atmospheric Research, 2005. PSU/NCAR Mesoscale Modelling System Tutorial Class Notes and User's Guide: MM5 Modelling System Version 3. NCAR, Boulder, Colorado.

Nemes A., Wösten, J.H.M. and Lilly A., 2001. Development of soil hydraulic pedotransfer functions on a European scale: their usefulness in the assessment of soil quality. Proc. 10th International Soil Conservation Organisation meeting, Purdue University.

Steffler P. and Blackburn J., 2002. River2D – Introduction to Depth Averaged Modelling and User's Manual. University of Alberta.

Svensson U., 2001. A continuum representation of fracture networks. Part 1: Method and basic test cases. J. Hydrology 250, 170-186.

Svensson U., 2001. A continuum representation of fracture networks. Part 2: Application to the Äspö Hard Rock laboratory. J. Hydrology 250, 187-205.

Yang C.T. and Simões F.J.M., 2000. User's Manual for GSTARS 2.1 (Generalised Stream Tube model for Alluvial River Simulation version 2.1). U.S. Department of the Interior Bureau of Reclamation. Denver, Colorado.

APPENDIX

A	River channel cross sectional area
A_d	Volume of bed sediment per unit channel length
A_s	Volume of suspended sediment per unit channel length
a	Upslope drainage area
C_s	Chezy coefficient
c_p	Specific heat capacity of air
D	Diffusion coefficients for the planetary boundary layer
E	Evapotranspiration rate
e_s	Saturated vapour pressure at temperature T_0

e_z	Vapour pressure at reference height in vegetation canopy	
f	Coriolis parameter	
	Froude number	equation (25)
g	Acceleration due to gravity	
H	Total energy available for evapotranspiration	
	River hydraulic head	equation (30)
	Flow depth	equation (33)
	Fracture plane extent in the z direction	equation (35)
h	Hydraulic head	
	Fracture thickness	equation (35)
K	Hydraulic conductivity of porous medium	
	River conveyance	equation (26)
K_s	Saturated hydraulic conductivity	
L	Fracture plane extent in the x direction	
M_t	Vertically integrated moisture convergence	
m	Map scale factor,	
	van Genuchten parameter for hydraulic conductivity of soil	equation (22)
N_h	Function for vertical profile of convective heating	
n	Manning roughness coefficient	
P_{CON}	Condensation of water vapour	
P_{ID}	Deposition of vapour onto ice crystals	
P_{II}	Initiation of ice crystals	
P_{RA}	Accretion of cloud drops by rain drops	
P_{RC}	Conversion of cloud drops to rain drops	
P_{RE}	Evaporation of rain drops	
p	Pressure	
p_s	Surface pressure	
p_t	Pressure at top of the model	
p*	p_s - p_t	
p_0	Reference pressure	
p'	Perturbation pressure	
Q	Diabatic cooling rate	
	River discharge	equation (25)
q_c	Cloud water mixing ratio	
q_r	Rain water mixing ratio	
q_s	Sediment inflow to river	
q_v	Water vapour mixing ratio	
q_x	X component of river discharge	
q_y	Y component of river discharge	
R	Hydraulic radius for river channel	
r_a	Evapotranspiration aerodynamic resistance of canopy	
r_c	Evapotranspiration stomatal resistance of canopy	
S	Water storage in porous medium	
S_0	Channel bottom slope	
T	Transmissivity of river bank material	
T'	Perturbation temperature	
T_z	Temperature at canopy reference height z	
t	Time	
U	Component of water velocity in y direction	
u	Wind velocity component eastwards	

V	Mean river velocity	
	Component of water velocity in x direction	equations (32-33)
V_f	Fall velocity for rain drops	
v	Wind velocity component northwards	
W	Drainage sources and sinks	
	Channel width	equation (25)
	Fracture plane extent in the y direction	equation (35)
w	Vertical air velocity	
x	Horizontal coordinate eastwards	
y	Horizontal coordinate northwards	
z	Vertical coordinate	
	Elevation of channel bed above datum	equation (24)
z_b	Ground surface elevation	
α	River cross-sectional velocity distribution coefficient	
β	Slope angle	
ε	Parameter of the eddy viscosity coefficient	
Φ_T	Total stream energy	
ϕ	Latitude	
γ	Ratio of heat capacities (c_p/c_v) for dry air	
	Psychrometric constant	equation (23)
	Specific weight of water	equation (29)
η	Volume of sediment in unit bed volume (1-porosity)	
ν_t	Eddy viscosity coefficient	
θ	Soil moisture content	
θ_s	Saturated soil moisture content	
θ_r	Residual soil moisture content	
ρ_a	Density of air	
ρ_0	Reference state density of air	
σ	Vertical coordinate of the atmospheric model	
$\dot{\sigma}$	Vertical air velocity in sigma coordinates	
ψ	Co-latitude = $90^0 - \phi$	